Testing coalescence and statistical-thermal production scenarios for (anti-)(hyper-)nuclei and exotic QCD objects at LHC energies

Francesca Bellini* and Alexander P. Kalweit†
European Organization for Nuclear Research (CERN)
Geneva, Switzerland
(Dated: September 27, 2018)

We present a detailed comparison of coalescence and thermal-statistical models for the production of (anti-)(hyper-)nuclei in high-energy collisions. For the first time, such a study is carried out as a function of the size of the object relative to the size of the particle emitting source. Our study reveals large differences between the two scenarios for the production of objects with extended wave-functions. While both models give similar predictions and show similar agreement with experimental data for (anti-)deuterons and (anti-)^{3}He nuclei, they largely differ in their description of (anti-)hyper-triton production. We propose to address experimentally the comparison of the production models by measuring the coalescence parameter systematically for different (anti-)(hyper-)nuclei in different collision systems and differentially in multiplicity. Such measurements are feasible with the current and upgraded LHC experiments. Our findings highlight the unique potential of ultra-relativistic heavy-ion collisions as a laboratory to clarify the internal structure of exotic QCD objects and can serve as a basis for more refined calculations in the future.

I. INTRODUCTION

Nuclei and hyper-nuclei are special objects with respect to non-composite hadrons (pions, protons, etc.), because their size is comparable to a fraction or the whole system created in high-energy proton-proton (pp), proton-nucleus (pA) and nucleus-nucleus (AA) collisions [1]. Their size is typically defined as the rms of their (charge) wave-function, corresponding to about 2 fm for light (anti-)nuclei as obtained from electron scattering experiments. For the hyper-triton, theoretical calculations indicate a rms of the wave-function of about 5 fm [2], significantly larger than that of non-strange nuclei with mass number $A = 3$ and driven by the average separation of the Λ with respect to the two other nucleons. The properties of the objects under study here are summarised in Tab. I.

For about sixty years, coalescence models have been used to describe the formation of composite objects [10–18]. Surprisingly, thermal-statistical models have been successful in describing also the production of light (anti-)(hyper-)nuclei across a wide range of energies in AA collisions [19, 20]. In this approach, particles are produced from a fireball in thermal and kinetic equilibrium with temperatures of the order of $T_{chem} \approx 156$ MeV. Particle abundances are fixed at chemical freeze-out, when inelastic collisions cease. Further elastic and pseudo-elastic collisions occur among the components of the expanding fireball, that can affect the spectral shapes and the measurable yields of short-lived (strongly decaying) hadronic resonances. Once the mean free path for elastic collisions is larger than the system size, the fireball freezes-out kinetically at $T_{kin} \approx 90$ MeV [23]. In such a dense and hot environment, composite objects with binding energies that are small with respect to the temperature of the system, appear as "fragile". For instance, the binding energy of the deuteron is $B_{E,d} = 2.2$ MeV $\ll T_{chem}, T_{kin}$. The cross-section for pion-induced deuteron breakup is significantly larger than the typical (pseudo)-elastic cross-sections for the re-scattering of hadronic resonance decay products [24–26]. Similarly, the elastic cross-section driving deuteron spectra to kinetic equilibration in central heavy-ion collisions [27] is smaller than the breakup cross-section [24–26]. The deuterons produced at chemical freeze-out would be expected not to survive the hadronic phase, yet their production is measured to be consistent with statistical-thermal model predictions and a non-zero elliptic flow is observed [27]. Several solutions have been proposed to solve this "light (anti-)nuclei puzzle": (a.) a sudden freeze-out at the QGP-hadron phase boundary, (b.) the thermal production of these objects as compact quark bags [19], and (c.) the coincidence of coalescence and thermal production [14, 28]. Data from rescattering of short-lived hadronic resonances suggest a long-lasting hadronic phase [29], thus strongly disfavouring hypothesis (a.). While hypothesis (b.) cannot presently be tested beyond the agreement of measured (anti-)nuclei yields with statistical-thermal model predictions, hypothesis (c.) is scrutinised in this letter.

To this purpose, we compare LHC data to models. For the first time, these data allow for the systematic study of the light (anti-)(hyper-)nuclei production as a function of the system- and object-size. A quantitative comparison of the two scenarios has been proposed in [30], resulting in the idea to study the production rates of nuclei with similar mass but very different internal structure, as ^{4}He and ^{4}Li [17]. However, as ^{4}Li is not stable with respect to strong decay, its measurement is experimentally difficult and probably less constraining than the comparison with the hyper-nuclei proposed here. We propose that B_A is systematically measured in all collision systems by ex-

* francesca.bellini@cern.ch
† alexander.kalweit@cern.ch

Mass number	Nucleus	Composition	Binding energy (MeV)	Spin	${\lambda_A}^{meas}$ (fm)	r_A (fm)	Refs.
A = 2	d	pn	2.224575 (9)	1	2.1413 ± 0.0025	3.2	[3, 4]
A = 3	^{3}H	pnn	8.4817986 (20)	1/2	1.755 ± 0.086	2.15	[5]
	^{3}He	ppn	7.7180428 (23)	1/2	1.959 ± 0.030	2.48	[5]
	$^3_\Lambda$H	pΛn	0.13 ± 0.05	1/2	4.9 – 10.0	6.8 – 14.1	[2, 6]

TABLE I. Properties of nuclei and hyper-nuclei with mass number $A \leq 3$. The nucleus size is given in terms of the (charge) rms radius of the wave-function, λ_A. The size parameter of the wave-function of the harmonic oscillator potential, r_A, is chosen such that the measured/expected rms, ${\lambda_A}^{meas}$ (fm), is approximately reproduced. The proton rms charge radius $\lambda_p = 0.879(8)$ fm [9] is subtracted from λ_A^{meas} according to $\lambda_A = \sqrt{(\lambda_A^{meas})^2 - \lambda_p^2}$ to account for the finite extension of the constituents. We assume $\lambda_\Lambda \approx \lambda_n \approx \lambda_p$.

ploiting the large statistics sample foreseen at the LHC Run 3 & 4, in order to discriminate the aforementioned scenarios.

II. COALESCENCE APPROACH

In the coalescence picture, nucleons produced in the collision coalesce into nuclei if they are close in space and have similar velocities [10, 11]. For a nucleus with mass number $A = Z + N$, the coalescence probability is quantified by the coalescence parameter B_A. Considering that at LHC energies the number of produced protons and neutrons at midrapidity is expected to be equal, B_A is defined as

$$E_A \frac{\mathrm{d}^3 N_A}{\mathrm{d}p_A^3} = B_A \left(E_{\mathrm{p,n}} \frac{\mathrm{d}^3 N_{\mathrm{p,n}}}{\mathrm{d}p_{\mathrm{p,n}}^3} \right)^A \Big|_{\vec{p}_\mathrm{p} = \vec{p}_\mathrm{n} = \frac{\vec{p}_A}{A}} . \quad (1)$$

where $p_{\mathrm{p,n}}$ are the momenta of the proton and neutron and $E_{p,n}$ their energies. The LHC is particularly suited for the production of anti-nuclei, since the number of baryons and anti-baryons is essentially equal at midrapidity [31]. Consequently, the anti-particle to particle ratio for (hyper-)nuclei is consistent with unity [27, 32–34].

In a simple coalescence approach, B_A is expected to be independent of momentum and of the object size relative to the volume of particle emission (hereafter referred to as "source volume" or "size"). While this picture is found to be approximately valid in pp and p–Pb collisions [32, 33], it breaks down in Pb–Pb collisions, which exhibit a strong decrease of B_A with centrality [35]. The elliptic flow of deuterons cannot be explained by simple coalescence [27].

More advanced coalescence models [12–14] take into account the source size, as the coalescence probability naturally decreases for nucleons with similar momenta that are produced far apart in configuration space. We rely on the formalism proposed in [14]. As coalescence is a quantum-mechanical process, the classical definition of phase space is replaced by the Wigner formalism. The production probability of a nucleon cluster is given by the overlap of the Wigner function with the phase-space distributions of the constituents. The wave-functions of the (hyper-)nuclei are approximated by the ground-state wave-functions of an isotropic spherical harmonic oscillator as in [14] with one single characteristic-size parameter, r_A. For the deuteron wave-function $\varphi_d(\vec{r})$, one obtains

$$\varphi_d(\vec{r}) = (\pi r_d^2)^{-3/4} \exp\left(-\frac{r^2}{2r_d^2}\right) . \quad (2)$$

For nuclei with $A > 2$, analogous forms exist. The relation between r_A and the rms of the wave-function was derived in [36] as

$$\lambda_A^2 = \frac{3}{2}\frac{A-1}{A}\frac{r_A^2}{2} \quad (3)$$

for point-like constituents. We follow the gaussian ansatz to obtain fully analytic solutions. In Tab. I, we list the measured rms of the wave-function, λ_A^{meas}, and the r_A parameter derived from these relations. We encourage future more rigorous numerical studies that address the calculation of coalescence probabilities with more realistic wave-functions, e.g. the Hulthen parameterisation for deuterons [13] or a Λ-deuteron parameterisation for hyper-tritons as done only for central collisions in [37].

The quantum-mechanical nature of the coalescence products is explicitly accounted for by means of an average correction factor, $\langle C_A \rangle$. For deuterons, $\langle C_d \rangle$ has been approximated as

$$\langle C_d \rangle \approx \frac{1}{\left[1 + \left(\frac{r_d}{2R_\perp(m_T)}\right)^2\right] \sqrt{1 + \left(\frac{r_d}{2R_\parallel(m_T)}\right)^2}} \quad (4)$$

where r_d is the size parameter, $R_\perp$ and $R_\parallel$ are the lengths of homogeneity of the coalescence volume and m_T is the transverse mass of the coalescing nucleons. The nucleus size enters in the calculation of B_2 via $\langle C_d \rangle$, as well as the homogeneity volume $R_\perp^2 R_\parallel$, according to the relation [14]

$$B_2 = \frac{3\pi^{3/2}\langle C_d \rangle}{2 m_T R_\perp^2(m_T) R_\parallel(m_T)} . \quad (5)$$

The coalescence parameter decreases with increasing volume, as expected. $\langle C_d \rangle$ introduces a length scale defined by the deuteron size relative to the source size. If we assume that $R_\perp \approx R_\parallel \approx R$, Eqs. 4 and 5 simplify to

$$\langle C_d \rangle \approx \left[1 + \left(\frac{r_d}{2R(m_T)}\right)^2\right]^{-3/2} \tag{6}$$

and

$$B_2 = \frac{3\pi^{3/2}\langle C_d \rangle}{2m_T R^3(m_T)}. \tag{7}$$

Figure 1 shows the source radius (R) dependence of $\langle C_d \rangle$ and B_2, calculated assuming (a.) $r_d = 0$, (b.) $r_d = 0.3$ fm, (c.) the actual value $r_d = 3.2$ fm [4], (d.) a larger, irrealistic $r_d = 10$ fm. As shown in Fig. 1, $\langle C_d \rangle$ suppresses significantly the production of objects with radius larger than the source.

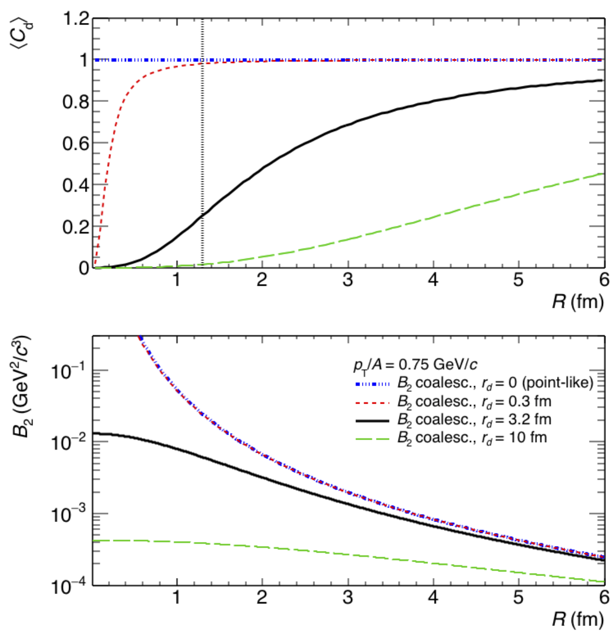

FIG. 1. The quantum-mechanical correction factor $\langle C_d \rangle$ (left panel, see Eq. 6) and the coalescence parameter B_2 for deuteron (right panel, see Eq. 7) as a function of the radius of the source R, calculated assuming a size parameter for the deuteron $r_d = 0, 0.3, 3.2$ and 10 fm. The inflection point of $\langle C_d \rangle$ corresponds to $R = r_d/\sqrt{6}$ and is indicated in the left panel by the vertical dotted line for $r_d = 3.2$ fm.

Following the discussion in [16], Eq. 4 may be generalised as

$$\langle C_A \rangle = \prod_{i=1,2,3} \left(1 + \frac{r^2}{4R_i^2}\right)^{-\frac{1}{2}(A-1)} \quad . \tag{8}$$

Similarly, the coalescence parameter B_A for a nucleus with mass number A and spin J_A is generalised by Eq. 6.2 of [14]. For the case of ^{3}He, the latter becomes Eq. 9 of [16].

In summary, under the assumption $R_1 \approx R_2 \approx R_3 \approx R$ as in [16] (see next section) and by combining Eq. 6.2 in [14] and Eq. 8, we obtain:

$$\boxed{B_A = \frac{2J_A+1}{2^A}\frac{1}{\sqrt{A}}\frac{1}{m_T^{A-1}}\left(\frac{2\pi}{R^2 + (\frac{r_A}{2})^2}\right)^{3/2(A-1)}} . \tag{9}$$

This general formula can be used to compare the predicted B_A with data directly.

For small sources, as $R \to 0$, the coalescence probability is anti-proportional to the harmonic oscillator size parameter, and thus proportional to the depth of the attractive potential in the harmonic oscillator picture (and thus to the nucleus binding energy). Quite naturally, the allowed momentum difference between the coalescing nucleons is larger for more attractive, i.e. deeper, potentials. For a large source, i.e. $R \gg r_A$, the coalescence probability is dominated by the classical phase-space separation, thus decreases for large distances in configuration space.

A. Source volume

We identify the source volume as the effective subvolume of the whole system that is governed by the homogeneity length of the interacting nucleons, as in [14], and experimentally accessible with Hanbury-Brown-Twiss (HBT) interferometry. Experimental results are typically obtained following the Bertsch-Pratt (BP) parameterisation ($R_{out}, R_{side}, R_{long}$), while the coalescence model described in Section II expresses the volume in terms of the Yano-Koonin-Podgoretskii (YKP) parameterisation. We identify $R_\perp = R_{side}$, $R_\parallel = R_{long}$ and then take $R = (R_\perp^2 R_\parallel)^{1/3} \approx (R_{side}^2 R_{long})^{1/3}$.

Experimentally, R can be controlled by selecting different collision geometries, i.e. different centrality classes [38]. The HBT radii scale with the cubic root of the average charged-particle multiplicity density $\langle \mathrm{d}N_{\mathrm{ch}}/\mathrm{d}\eta \rangle^{1/3}$ [1], and depend on the pair average transverse momentum $\langle k_{\mathrm{T}} \rangle$ [39]. We make the simplifying assumption that the scaling with $\langle \mathrm{d}N_{\mathrm{ch}}/\mathrm{d}\eta \rangle^{1/3}$ holds across collision systems, which is approximately fulfilled in data [40]. In contrast to [16], we do not explicitly use the measured HBT radii in our study, but we derive$R$ from the measured $\langle \mathrm{d}N_{\mathrm{ch}}/\mathrm{d}\eta \rangle$ according to the following:

$$R = a\,\langle \mathrm{d}N_{\mathrm{ch}}/\mathrm{d}\eta \rangle^{1/3} + b \quad . \tag{10}$$

The coefficients, $a = 0.339$ and $b = 0.128$ (in units of fm), have been determined by fitting linearly the ALICE data, as shown in Fig. 2. The values we obtain by interpolating the geometric mean of the measured radii are consistent with the radii from kaon femtoscopy for $m_{\rm T} \approx 1$ GeV/c in low-multiplicity pp collisions [41] and the radii from pion femtoscopy in high-multiplicity Pb–Pb collisions at the highest available $k_{\rm T} \approx 0.9$ GeV/c [1]. The highest $k_{\rm T}$ was chosen as it is closest in $m_{\rm T}$ to the lowest transverse momentum per nucleon ($p_{\rm T}/A \approx 0.8$ GeV/c) accessible by ALICE for the measurement of nuclei production. Ideally, one would use the proton femtoscopic radii, but given the unavailability of these measurements in every collision system and centrality, we assume that $m_{\rm T}$-scaling holds[42].

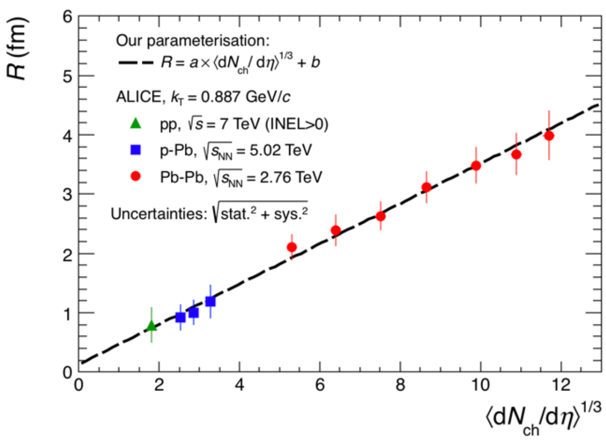

FIG. 2. Parameterisation A of the dependence of the source radius on multiplicity compared to HBT data from [1, 40, 41]. The radius R and the parameters a and b are in units of fm.

III. STATISTICAL-THERMAL APPROACH AND BLAST-WAVE

In the statistical-thermal approach [44–46], the yields (dN/dy) of light anti- and hyper-nuclei are very sensitive to T_{chem} due to their large mass and approximately scale as $dN/dy \propto \exp(-m/T_{chem})$. At the LHC, the chemical potentials which ensure the conservation of baryon number, strangeness, and electric charge are negligible. In contrast to coalescence, the statistical-thermal models provide only $p_{\rm T}$-integrated yields. We use a blast-wave [47] parameterization to model the $p_{\rm T}$-dependence, with parameters obtained from the simultaneous fit to pion, kaon and proton spectra measured in Pb–Pb collisions by ALICE [23]. The normalisation is fixed using the $p_{\rm T}$-integrated deuteron-to-pion ratio and ^{3}He-to-pion ratio predicted by the GSI-Heidelberg model with $T_{chem} = 156$ MeV, multiplied by the measured pion yield [23]. This choice, as opposed to using the ratio to proton, is motivated by the fact that the measured proton yield is seen to be slightly overestimated by the thermal model [48]. For hyper-triton, the normalisation is extracted from the statistical-thermal model prediction of the strangeness population factor $S_3 = \frac{^3_\Lambda{\rm H}/^3{\rm He}}{\Lambda/p}$ multiplied by the measured Λ/p ratio [23, 49] and ^{3}He yield [35]. With the resulting spectra, we calculate B_A for a given $p_{\rm T}/A$ and compare it with coalescence expectations. We use the corresponding $\langle dN_{\rm ch}/d\eta \rangle$ in each class to estimate the system radius based on the parameterisation discussed in Sec. II A. In contrast to the coalescence approach, the object size does not enter in the formulation of the blast-wave model. The thermal model on the other hand, implements eigenvolume corrections by fixing the object radius as an external parameter. We refer to the literature for the extensive discussions on the validity of the eigenvolume correction for light (anti-)(hyper-)nuclei [50] and the relation with the possible production as compact quark bags [19].

IV. CONSTRAINING THE SOURCE VOLUME WITH DATA

Multiplicity-differential data on anti- and hyper-nuclei production at the LHC have been released by ALICE [27, 32, 34, 35]. To facilitate the comparison with multiplicity-dependent data given in the INEL>0 class, we have rescaled the inelastic pp collision data in [32] by the ratio of $\langle dN_{\rm ch}/d\eta \rangle$ in these two event classes [51]. In order to map $\langle dN_{\rm ch}/d\eta \rangle$ to the source size we first used the parameterisation (labeled as "A") from the fit to the HBT data shown in Fig. 2. When comparing to data, we found a discrepancy between the coalescence volume from parameterisation A and the coalescence curve. In particular, the model would require a larger radius for a given value of B_2 in Pb–Pb collisions. In a second step we tuned the parameterisation (labeled as "B") such that the data points for (anti-)deuterons fall onto the coalescence prediction, finding the values $a = 0.473$ and $b = 0$ for Eq. 10.

With parameterisation B, we compare models to data, thus constraining the coalescence volume with the more differential (anti-)deuteron data and assuming that it is the same for all anti- and hyper-nuclei. The necessity of introducing a second parameterisation might suggest that the kinetic freeze-out volume relevant for coalescence is not given by the m_T-scaled pion HBT radius considered in parameterisation A, but by a slightly larger system as from parameterisation B.

V. COMPARISON WITH DATA

In Fig. 3, the available data for (anti-)deuterons, (anti-)^{3}He and (anti-)$^3_\Lambda$H [34] are compared to coalescence and to the thermal model+blast wave predictions described in Sec. III. For the latter and for data, the radius parameterisation B is used, see Sec. IV. For deuterons, both approaches lead to similar predictions and give a reasonable description of the experimental data for $R \gtrsim 1.6$ fm. For ^{3}He the two models exhibit a qualitatively similar trend as a function of R, but they differ by a factor of about 1.5 to 2. The limited amount of data that is currently available is consistent with both models within 2σ to 3σ, where σ is the total uncertainty on the data. Both approaches show large differences (a factor 5 to 6 for central Pb–Pb collisions and a factor larger than 50 for small radii, $R < 2$ fm) for the ${}^{3}_{\Lambda}\mathrm{H}$ caused by the significantly larger size of ${}^{3}_{\Lambda}\mathrm{H}$ with respect to ${}^{3}\mathrm{He}$. The only data point available so far in Pb–Pb collisions is in agreement with the thermal model but not with coalescence. The difference between data and the coalescence model is about 6σ, albeit the validity of our assumptions (*in primis* the usage of a gaussian wave-function). In [37] it is argued that the difference between data and the coalescence model might be explained by a later formation through the coalescence of Λs and deuterons. A possible difference attributable to the presence of excited states with $J = 3/2$ of ${}^{3}_{\Lambda}\mathrm{H}$, which would significantly enhance the phase space for its production, is not considered here as there is no evidence for its existence [52].

Most importantly, Fig. 3 shows that the difference between the two approaches increases with decreasing source volume, thus underlining the need for additional and more precise data as a function of multiplicity in order to distinguish between the two production scenarios. In the case of ${}^{3}_{\Lambda}\mathrm{H}$ we have considered also a prediction from coalescence for a wider wave-function (dashed line in bottom right panel of Fig. 3), which results in even lower production probabilities. This behaviour highlights the unique potential to constrain the wave-function of the particle under study at the moment of its production via precise measurements of the coalescence parameter as a function of the source volume. The curves presented here also explicitly allow for an estimate of the expected hyper-triton production in pp collisions, which is expected to be suppressed by about two orders of magnitude with respect to the production of ${}^{3}\mathrm{He}$, thus making this measurement a prime candidate for future experimental studies.

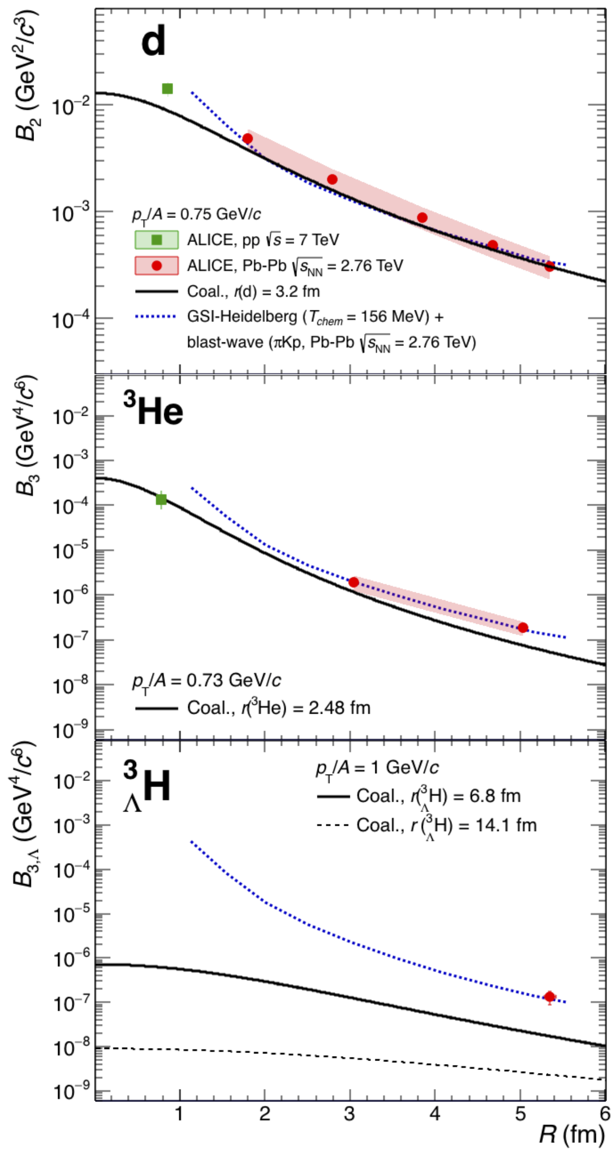

FIG. 3. Comparison of the coalescence parameters measured by ALICE (solid markers) for deuterons (upper panel), ${}^{3}\mathrm{He}$ (middle panel) and ${}^{3}_{\Lambda}\mathrm{H}$ (lower panel) in pp [32] and Pb–Pb [34, 35] collisions with the thermal+blast-wave model expectations (dotted line) and the coalescence predictions (solid lines). Parameterisation B has been used to map $\langle \mathrm{d}N_{\mathrm{ch}}/\mathrm{d}\eta \rangle$ into the radius R of the source. The dashed line in the lower right panel corresponds to the coalescence prediction for the ${}^{3}_{\Lambda}\mathrm{H}$ with a larger radius.

VI. CONCLUSIONS AND OUTLOOK

We summarise our main conclusions as follows:

1. For the production of $A = 2$ and $A = 3$ (anti-)nuclei in heavy-ion collisions, the thermal and coalescence models give similar predictions for a source volume that is constrained by experimental data on d, $\bar{\mathrm{d}}$ production in central Pb–Pb collisions at the LHC.

2. For the production of hyper-triton, the thermal and coalescence models give very different predictions as a function of source volume. In particular, the yield of hyper-triton appears to be suppressed by about two orders of magnitude in pp collisions with respect to the production of ${}^{3}\mathrm{He}$. The very limited amount of currently available data favours the thermal model prediction within our assumptions.

3. Systematic measurements in pp, p–Pb, and Pb–Pb collisions at LHC energies have a unique potential to clarify the production mechanism and the nature of composite QCD objects. Ideally, such

measurements are accompanied by systematic measurements of the HBT radii in the same multiplicity/centrality classes and collision systems.

As our study is deliberately based on simplified assumptions that allow for a completely analytical treatment of the problem, future studies should be based on more realistic approximations (in particular the wave-function), which require numerical calculations. Moreover, it will be interesting to explore further the p_{T} dependence of the observations made here.

In a follow-up publication, we plan to extend our study to predictions for the $A = 4$ systems introduced in Tab. I and to more exotic QCD objects like the X(3872) [15, 53]. In fact, if the X(3872) corresponds to a loosely bound $\overline{D}^{*0}$–D^0 molecule, the rms of its wave-function can be as large as $4.9^{+13.4}_{-1.4}$ fm [54]. Thus, its possible production via a coalescence mechanism in pp collisions would be subject to a similar suppression as the hyper-triton. The upcoming high-luminosity phase of the LHC (Run 3 & 4), where $A = 4$ hyper-nuclei and other rare composite objects will become experimentally accessible, will provide a unique opportunity for the final understanding of (anti-)(hyper-)nuclei production. Setting a final word on the production mechanisms also has a broader application in astrophysics and dark-matter searches, by representing an essential input for the measurement of (anti-)nuclei in space with ongoing [55, 56] and future [57, 58] experiments.

ACKNOWLEDGMENTS

We would like to thank Kfir Blum for inspiring this work. We thank U. Heinz for the useful discussions and the clarification on the equivalence of the Bertsch-Pratt and Yano-Koonin-Podgoretskii parameterisations of the HBT radii. We further acknowledge discussions with Benjamin Doenigus, in particular about the production of ${}^{3}_{\Lambda}$H in pp collisions, and with Eulogio Serradilla Rodriguez. In addition, we would like to thank Juergen Schukraft, Peter Braun-Munzinger, Marco Van Leuween, Maximiliano Puccio, Roman Lietava, Natasha Sharma and the colleagues from the ALICE Collaboration for their valuable input.

[1] J. Adam *et al.* (ALICE), Phys. Rev. **C93**, 024905 (2016), arXiv:1507.06842 [nucl-ex].
[2] H. Nemura, Y. Suzuki, Y. Fujiwara, and C. Nakamoto, Prog. Theor. Phys. **103**, 929 (2000), arXiv:nucl-th/9912065 [nucl-th].
[3] C. Van Der Leun and C. Alderliesten, Nucl. Phys. **A380**, 261 (1982).
[4] P. J. Mohr, D. B. Newell, and B. N. Taylor, Rev. Mod. Phys. **88**, 035009 (2016), arXiv:1507.07956 [physics.atom-ph].
[5] J. E. Purcell and C. G. Sheu, Nucl. Data Sheets **130**, 1 (2015).
[6] D. H. Davis, *Proceedings on 8th International Conference on Hypernuclear and strange particle physics (HYP 2003): Newport News, USA, October 14-18, 2003*, Nucl. Phys. **A754**, 3 (2005).
[7] M. Wang, G. Audi, F. Kondev, W. Huang, S. Naimi, and X. Xu, Chinese Physics C **41**, 030003 (2017).
[8] I. Angeli and K. P. Marinova, Atom. Data Nucl. Data Tabl. **99**, 69 (2013).
[9] J. C. Bernauer *et al.* (A1), Phys. Rev. Lett. **105**, 242001 (2010).
[10] S. T. Butler and C. A. Pearson, Phys. Rev. **129**, 836 (1963).
[11] J. I. Kapusta, Phys. Rev. **C21**, 1301 (1980).
[12] H. Sato and K. Yazaki, Phys. Lett. **B98**, 153 (1981).
[13] J. L. Nagle, B. S. Kumar, D. Kusnezov, H. Sorge, and R. Mattiello, Phys. Rev. **C53**, 367 (1996).
[14] R. Scheibl and U. W. Heinz, Phys. Rev. **C59**, 1585 (1999), arXiv:nucl-th/9809092 [nucl-th].
[15] S. Cho *et al.* (ExHIC), Prog. Part. Nucl. Phys. **95**, 279 (2017), arXiv:1702.00486 [nucl-th].
[16] K. Blum, K. C. Y. Ng, R. Sato, and M. Takimoto, Phys. Rev. **D96**, 103021 (2017), arXiv:1704.05431 [astro-ph.HE].
[17] S. Bazak and S. Mrowczynski, (2018), arXiv:1802.08212 [nucl-th].
[18] W. Zhao, L. Zhu, H. Zheng, C. M. Ko, and H. Song, (2018), arXiv:1807.02813 [nucl-th].
[19] A. Andronic, P. Braun-Munzinger, K. Redlich, and J. Stachel, (2017), arXiv:1710.09425 [nucl-th].
[20] A. Andronic, P. Braun-Munzinger, J. Stachel, and H. Stocker, Physics Letters B **697**, 203 (2011).
[21] A. Bazavov *et al.* (HotQCD), Phys. Rev. **D90**, 094503 (2014), arXiv:1407.6387 [hep-lat].
[22] R. Bellwied, S. Borsanyi, Z. Fodor, S. D. Katz, and C. Ratti, Phys. Rev. Lett. **111**, 202302 (2013), arXiv:1305.6297 [hep-lat].
[23] B. Abelev *et al.* (ALICE), Phys. Rev. **C88**, 044910 (2013), arXiv:1303.0737 [hep-ex].
[24] H. Garcilazo, Phys. Rev. Lett. **48**, 577 (1982).
[25] S. A. Bass *et al.*, Prog. Part. Nucl. Phys. **41**, 255 (1998), arXiv:nucl-th/9803035 [nucl-th].
[26] J. Schukraft, *Proceedings, 26th International Conference on Ultra-relativistic Nucleus-Nucleus Collisions (Quark Matter 2017): Chicago, Illinois, USA, February 5-11, 2017*, Nucl. Phys. **A967**, 1 (2017), arXiv:1705.02646 [hep-ex].
[27] S. Acharya *et al.* (ALICE), Eur. Phys. J. **C77**, 658 (2017), arXiv:1707.07304 [nucl-ex].
[28] U. Heinz, "Coalescence model involving HBT and flow," Presentation at EMMI Workshop in Torino, November 2017.
[29] B. B. Abelev *et al.* (ALICE), Phys. Rev. **C91**, 024609 (2015), arXiv:1404.0495 [nucl-ex].
[30] S. Mrowczynski, Acta Phys. Polon. **B48**, 707 (2017), arXiv:1607.02267 [nucl-th].
[31] E. Abbas *et al.* (ALICE), Eur. Phys. J. **C73**, 2496 (2013),

arXiv:1305.1562 [nucl-ex].
[32] S. Acharya *et al.* (ALICE), Phys. Rev. **C97**, 024615 (2018), arXiv:1709.08522 [nucl-ex].
[33] Anielski, Jonas, *Proceedings, Hot Quarks 2014: Workshop for young scientists on the physics of ultrarelativistic nucleus–nucleus collisions, Andalucia, Spain*, J. Phys. Conf. Ser. **612**, 012014 (2015).
[34] J. Adam *et al.* (ALICE), Phys. Lett. **B754**, 360 (2016), arXiv:1506.08453 [nucl-ex].
[35] J. Adam *et al.* (ALICE), Phys. Rev. **C93**, 024917 (2016), arXiv:1506.08951 [nucl-ex].
[36] A. Shebeko, P. Papakonstantinou, and E. Mavrommatis, Eur. Phys. J. **A27**, 143 (2006), arXiv:nucl-th/0602056 [nucl-th].
[37] Z. Zhang and C. M. Ko, Phys. Lett. **B780**, 191 (2018).
[38] B. Abelev *et al.* (ALICE), Phys. Rev. **C88**, 044909 (2013), arXiv:1301.4361 [nucl-ex].
[39] K. Aamodt *et al.* (ALICE), Phys. Lett. **B696**, 328 (2011), arXiv:1012.4035 [nucl-ex].
[40] J. Adam *et al.* (ALICE), Phys. Rev. **C91**, 034906 (2015), arXiv:1502.00559 [nucl-ex].
[41] B. Abelev *et al.* (ALICE), Phys. Rev. **D87**, 052016 (2013), arXiv:1212.5958 [hep-ex].
[42] J. Adam *et al.* (ALICE), Phys. Rev. **C92**, 054908 (2015), arXiv:1506.07884 [nucl-ex].
[43] A. Kisiel, M. Galazyn, and P. Bozek, Phys. Rev. **C90**, 064914 (2014), arXiv:1409.4571 [nucl-th].
[44] M. Petran, J. Letessier, J. Rafelski, and G. Torrieri, Comput. Phys. Commun. **185**, 2056 (2014), arXiv:1310.5108 [hep-ph].
[45] S. Wheaton and J. Cleymans, Comput. Phys. Commun. **180**, 84 (2009), arXiv:hep-ph/0407174 [hep-ph].
[46] A. Andronic, P. Braun-Munzinger, and J. Stachel, Nucl. Phys. **A772**, 167 (2006), arXiv:nucl-th/0511071 [nucl-th].
[47] E. Schnedermann, J. Sollfrank, and U. W. Heinz, Phys. Rev. **C48**, 2462 (1993), arXiv:nucl-th/9307020 [nucl-th].
[48] B. Abelev *et al.* (ALICE), Phys. Rev. Lett. **109**, 252301 (2012), arXiv:1208.1974 [hep-ex].
[49] B. B. Abelev *et al.* (ALICE), Phys. Rev. Lett. **111**, 222301 (2013), arXiv:1307.5530 [nucl-ex].
[50] V. Vovchenko and H. Stoecker, *Proceedings, 16th International Conference on Strangeness in Quark Matter (SQM 2016): Berkeley, California, United States*, J. Phys. Conf. Ser. **779**, 012078 (2017), arXiv:1610.02346 [nucl-th].
[51] J. Adam *et al.* (ALICE), Eur. Phys. J. **C77**, 33 (2017), arXiv:1509.07541 [nucl-ex].
[52] T. Mart, L. Tiator, D. Drechsel, and C. Bennhold, Nucl. Phys. **A640**, 235 (1998), arXiv:nucl-th/9610038 [nucl-th].
[53] A. Esposito, A. L. Guerrieri, L. Maiani, F. Piccinini, A. Pilloni, A. D. Polosa, and V. Riquer, Phys. Rev. **D92**, 034028 (2015), arXiv:1508.00295 [hep-ph].
[54] P. Artoisenet and E. Braaten, Phys. Rev. **D83**, 014019 (2011), arXiv:1007.2868 [hep-ph].
[55] J. Alcaraz *et al.* (AMS), Phys. Lett. **B461**, 387 (1999), arXiv:hep-ex/0002048 [hep-ex].
[56] V. Poulin, P. Salati, I. Cholis, M. Kamionkowski, and J. Silk, (2018), arXiv:1808.08961 [astro-ph.HE].
[57] S. Schael, "AMS-100 - A Magnetic Spectrometer at Lagrange Point 2," Presentation at AMS days La Palma, April 2018.
[58] T. Aramaki, C. J. Hailey, S. E. Boggs, P. von Doetinchem, H. Fuke, S. I. Mognet, R. A. Ong, K. Perez, and J. Zweerink (GAPS), Astropart. Phys. **74**, 6 (2016), arXiv:1506.02513 [astro-ph.HE].
[59] U. A. Wiedemann and U. W. Heinz, Phys. Rept. **319**, 145 (1999), arXiv:nucl-th/9901094 [nucl-th].